ELSEVIER

Chemical Geology 164 (2000) 21–34

CHEMICAL GEOLOGY
INCLUDING
ISOTOPE GEOSCIENCE

www.elsevier.com/locate/chemgeo

Magnetite–melt HFSE partitioning

Roger L. Nielsen [a,*], James S. Beard [b]

[a] College of Oceanic and Atmospheric Sciences, Oceanography Administration 104, Oregon State University, Corvallis, OR 97331-5503, USA

[b] Virginia Museum of Natural History, 1001 Douglas Ave., Martinsville, VA, 24112, USA

Received 20 August 1998; accepted 31 May 1999

Abstract

Results from doped, hydrous experiments on natural mafic-to intermediate-composition lavas at 2–5 kbar pressure were combined with existing 1 atm data to evaluate the effects of composition and temperature on the partitioning behavior of the high field strength elements (HFSE), Zr, Nb, Ta and Hf between magnetite and natural silicate melts. Magnetite composition was found to be the strongest controlling factor on partitioning behavior. The partition coefficients (D) for Zr, Nb, Hf, and Ta correlate with D_{Ti}, Ti and Al content of the magnetite, temperature and pressure. The partition coefficients for the HFSE are similar to one another for any given magnetite–melt pair, but range from < 0.02 in Cr, Al-rich magnetites and chromites to > 2 in titanomagnetite. In addition, the relationship between Ti and the HFSE changes as a function of pressure and temperature, with the HFSE becoming more incompatible relative to Ti at lower temperatures and/or higher pressures. This change in the relationship between D_{Ti} and D_{HFSE} with temperature and pressure means that the expressions presented in Nielsen et al. (1994) [Nielsen, R.L., Forsythe, L.M., Gallaghan, W.E., Fisk, M.R., 1994. Major and trace element magnetite–melt partitioning. Chem. Geol. 117, 167–191.] are not valid for hydrous, aluminous systems. Expressions were derived to describe the relationship between D_{HFSE} and temperature, pressure, Fe^{2+}/Mg exchange, Ti/Al ratio of the magnetite, and D_{Ti}. These expressions reproduce the input data within 35–50% (1σ) over a range extending from highly incompatible to compatible (< 0.02–3.0). This internal precision represents ~ 3–4% of the observed range of partition coefficients. These patterns of behavior are consistent with the observed miscibility gap between the Al, Cr spinel group end members and ülvospinel and magnetite.

Keywords: Magnetite; Partition coefficients; Experimental petrology; High field strength elements

1. Introduction

Experimental studies of mineral–melt equilibria as a function of temperature, pressure, and composition have gone a long way towards describing the controls on the partitioning of major, minor and trace elements in natural magmas. However, the development of any model of igneous differentiation requires a quantitative understanding of the nature of the interdependence of major and trace element behavior in compositionally complex natural systems. This in turn requires extensive experimental data from a wide range of conditions and phase compositions.

* Corresponding author. fax: +1-541-737-2064; e-mail: rnielsen@oce.orst.edu

0009-2541/00/$ - see front matter
PII: S0009-2541(99)00139-4

A knowledge of the processes involving spinel-group minerals in magmatic differentiation is required for the analysis of processes as diverse as magnetite fractionation in arc rocks (e.g., Gill, 1978; Sisson and Grove, 1993) and the role of spinel in mantle melting (e.g., Kelemen et al., 1990). This investigation focuses on the experimental determination of the systematics of the partitioning behavior of the high field strength elements (HFSE; Ti, Zr, Nb, Hf, Ta) between magnetite-rich spinels and a wide variety of natural composition silicate melts. We use the experimental data reported here, together with published data, to identify and quantify the parameters controlling magnetite–melt trace element equilibria.

The present work builds on the results of Nielsen et al. (1994), which reported the importance of the major element composition of spinel in determining trace element partitioning behavior at 1 atm. However, these 1 atm experiments represent only a small fraction of possible situations where magnetite is geologically important.

The range of reported trace element partition coefficients for the spinel-group minerals covers more than two orders of magnitude for many elements (Villemant et al., 1981; Worner et al., 1983; Lemarchand et al., 1987; Villemant, 1988; LaTourrette et al., 1991; Nielsen et al., 1992; Horn et al., 1994; Nielsen et al., 1994). Quantification of this diversity requires both knowledge of the controls on partitioning, and an adequate database on which to calibrate the expressions. Therefore, we have conducted a series of water-saturated experiments at 2 and 5 kbar on basaltic and andesitic starting compositions to investigate partitioning for liquid compositions ranging from andesite to tonalite and low-Si rhyolite.

2. Experimental procedure

2.1. Starting compositions

Natural starting compositions were chosen for this study (Table 1) to produce a wide range of melt compositions. Each starting material was powdered and doped with approximately 0.5 wt.% each of the dopant mixtures. The mixes were subsequently fused at 1 atm, 1200°C, quenched, ground, re-fused and re-ground. Three different dopant mixtures [(1) LLH — La, Lu, Hf; (2) NST — Nb, Sm, Ta; and (3) YZG — Y, Zr, Gd] were used in order to avoid interferences during microprobe analysis, and to keep concentrations sufficiently low to inhibit trace phase formation. Dopant mixtures were formulated using SpecPure oxides.

Table 1
Starting compositions used in this study
T85 — fractionated alkaline basalt from Tahiti T85 (Duncan et al., 1995). AT4 — high-alumina basalt from the Aleutian Islands (Beard and Lofgren, 1991). 557 — low-K calc-alkaline andesite (Beard and Lofgren, 1991). 478 — greenstone of arc tholeiitic basalt composition (Beard and Lofgren, 1991). ABA — Alkali basaltic amphibolite (Rushmer, 1991).

	T85	AT4	557	478	ABA
SiO_2	45.50	48.62	57.02	52.47	49.04
TiO_2	4.11	0.91	0.60	1.74	1.27
Al_2O_3	15.04	17.38	15.39	15.29	16.37
Fe_2O_3	13.84	6.21	–	–	1.92
FeO	–	4.19	8.01	11.79	7.45
MnO	0.18	0.13	0.17	0.22	0.18
MgO	5.12	7.66	5.52	5.29	7.45
CaO	10.95	11.64	9.20	9.21	10.81
Na_2O	3.5	2.44	2.54	2.55	3.42
K_2O	1.85	0.63	0.44	0.16	0.44
P_2O_5	0.14	0.19	0.18	0.49	0.16

2.2. Use of dopants

Experimental determination (versus phenocrysts/matrix) of partition coefficients offers the advantages that pressure and temperature are controlled. However, the size of crystals generated with experimental techniques is often small ($\sim$3–10 μ) and difficult to analyze by available analytical equipment (e.g., ion probe) capable of detecting trace elements in natural abundances. These problems can be addressed by doping an experiment with the elements of interest to levels that permit the use of an electron microprobe for in situ analysis of small crystals. The benefit of in situ analysis is that inclusions of trace phases can be detected and avoided with back scatter imaging and contamination of analyses by trace phases can be avoided (Michael, 1988). The amount of dopant added to our charges (0.5 wt.%), is enough to be measured by the electron microprobe, yet sufficiently dilute to fall within the

bounds of Henry's Law behavior (Drake and Holloway, 1981; Watson, 1985; Gallahan and Nielsen, 1992; Beattie, 1993). Detailed discussions of the validity of the Henry's Law approach in other mineral systems can be found in Nielsen et al. (1994) and Beattie (1993). However, to date, no investigation has been done on Henry's Law for magnetite.

2.3. Experimental technique

The experiments were conducted at Virginia Polytechnic Institute and State University and Oak Ridge National Laboratories in internally-heated pressure vessels (IHPV). Run times were 70–100 h. All experiments conducted at VPI were run in 100% argon pressure medium, with pressure (± 0.1 kbar) monitored by a manganin cell and temperature (± 7°C) monitored by three chromel–alumel thermocouples. Oxygen fugacity was not buffered or monitored, but in such systems it is typically about 1 log unit above the Nickel–Nickel Oxide (NNO) buffer (e.g., Patiño-Douce and Beard, 1995). The experiments conducted at Oak Ridge were run in a reducing environment of 96% argon and 4% hydrogen, equivalent to an oxygen fugacity of QFM-1. Pressure was monitored by calibrated Heise gauge and temperature by type-S thermocouples.

For each IHPV experiment, approximately 10–30 mg of powdered starting material with enough water to saturate (~ 10 wt. H_2O) was loaded into gold capsules. All charges were weighed before and after the experiment and all yielded fluid upon opening. Experiments were brought to run temperature with minimal overshoot, and quenched by turning the power off. Quench time was approximately 20–40 s.

2.4. Analytical technique

Major, minor and trace element analyses were conducted with the CAMECA SX-50 four-spectrometer electron microprobe at Oregon State University. Analysis of the magnetite crystals was performed with a 15 kV accelerating voltage and a 50 nA beam current. Glass analyses were conducted with a partially defocused beam (~ 5–10 μm) and a 10-nA beam current on Na to mitigate migration during analysis. The rest of the elements in the glass were analyzed at 30 nA. Peak counting times were 10 s on major and minor elements, 60 s for Ti, and 300 s for the trace elements. Original Na concentration levels in the glasses were estimated by extrapolating the rate of sodium loss back to time zero as described in Nielsen and Sigurdsson (1981).

Major elements were calibrated with Smithsonian standard reference materials (Jarosewich et al., 1980). The trace elements, Y, Nb, La, Lu and Ta were calibrated on a synthetic standard (Hfrest — Patiño-Douce et al., 1994). Hf and Zr were calibrated on the USNHM Zircon standard (117288-3), while Sm and Gd were calibrated using the REE standard of Drake and Weill (1972).

The experimental approach applied in these experiments resulted in small homogeneous crystals surrounded by glass. However, the areas of glass ranged up to 20 μ in diameter, precluding application of microanalytical techniques for the direct determination of water content. Water contents of the glass in each charge were estimated as the difference between Na-corrected microprobe total and 100 (Anderson, 1974; Garcia et al., 1979; Beard and Lofgren, 1991). Point acquisition was documented on backscattered electron images (BSE). Glass analyses are averages of a number of point analyses in each of several glass patches in each charge (Table 2).

One of the concerns during analysis of these experiments was that the beam sampling volume may be larger than the volume of a single small magnetite crystal, or glass patch. Any wandering of the beam off of the crystal during analysis will result in the fluorescence of more than one phase, creating a ''hybrid'' analysis of glass and magnetite. To identify such erroneous results, Si, K and P were added to the analytical routine for magnetite. Because the excitation volumes for these elements are at least as large as those for the HFSE, this combination of elements was found to be sufficient to discriminate between analyses of a single phase and analyses of more than one phase.

3. Magnetite crystal chemistry

The general formula for the spinel group may be expressed as AB_2O_4. Cations in the A site are in 4-fold co-ordination, while those in the B site are in

Table 2
Electron microprobe analyses of experimentally produced magnetite and glass
LLH — La, Lu, Hf; NST — Nb, Sm, Ta; YZG — Y, Zr, Gd. *n* — number of analyses on which the average is based.

	ABALLH	AT4LLH	557LLH	T85LLH	T85LLH
P (kbar)	5	5	5	2	2
T (°C)	940	940	940	945[a]	940
Magt *n*	12	9	6	9	12
SiO_2	0.14 (1)	0.15 (2)	0.13 (0)	0.15 (1)	0.13 (1)
TiO_2	4.94 (28)	3.83 (11)	3.17 (16)	4.07 (10)	8.07 (40)
Al_2O_3	5.24 (21)	4.37 (16)	6.05 (13)	3.60 (11)	4.53 (17)
Cr_2O_3	0.17 (1)	0.15 (1)	0.66 (2)	0.38 (5)	0.02 (0)
Fe_2O_3	53.93 (79)	56.03 (59)	57.32 (21)	56.63 (43)	50.34 (30)
FeO	31.26 (29)	30.86 (43)	26.70 (31)	30.06 (22)	30.99 (34)
MnO	0.41 (3)	0.43 (4)	0.30 (3)	0.36 (2)	0.43 (3)
MgO	2.82 (3)	2.03 (14)	5.02 (2)	2.76 (7)	4.94 (20)
CaO	0.26 (3)	0.34 (4)	0.21 (4)	0.22 (3)	0.19 (3)
H f_{O_2}	0.026 (5)	0.048 (5)	0.031 (2)	0.033 (7)	0.040 (15)
Total	99.20 (21)	98.24 (77)	99.59 (71)	98.27 (30)	99.68 (55)
Min. prop.	50 0 2 48	35 20 5 40	20 10 2 68	50 0 5 45	40 20 10 30
Glass *n*	29	12	15	12	19
SiO_2	59.32 (65)	61.17 (94)	63.71 (86)	61.18 (56)	56.00 (55)
TiO_2	0.33 (6)	0.23 (4)	0.27 (7)	0.61 (19)	1.01 (21)
Al_2O_3	19.53 (32)	18.18 (28)	17.15 (18)	19.55 (22)	19.01(11)
FeO	1.44 (32)	1.14 (20)	1.73 (19)	1.56 (19)	1.83 (21)
MnO	0.11 (3)	0.12 (3)	0.08 (3)	0.10 (2)	0.13 (2)
MgO	0.15 (13)	0.07 (11)	0.29 (25)	0.05 (3)	0.15 (1)
CaO	6.48 (16)	5.42 (16)	5.19 (14)	3.50 (23)	4.43 (17)
K_2O	0.22 (4)	0.55 (5)	0.27 (9)	1.42 (36)	2.78 (28)
Na_2O	4.44 (67)	3.77 (37)	3.41 (21)	4.73 (61)	3.57 (33)
P_2O_5	0.31 (5)	0.33 (5)	0.13 (3)	0.23 (7)	0.44 (7)
La_2O_3	0.73 (8)	0.24 (8)	0.18 (2)	0.32 (6)	0.72 (6)
Lu_2O_3	0.21 (2)	0.18 (3)	0.21 (5)	0.16 (4)	0.59 (4)
H f_{O_2}	0.35 (5)	0.29 (4)	0.19 (3)	0.33 (6)	0.35 (2)
Total	93.62 (55)	91.69 (55)	92.81 (81)	93.74 (28)	91.01 (39)

	ABANST	478NST	AT4NST	557NST	T85NST	AT4NST
P (kbar)	5	5	5	5	2	2
T (°C)	940	940	940	940	945[a]	940
Magt *n*	13	14	11	10	9	13
SiO_2	0.61 (10)	0.09 (2)	0.10 (2)	0.24 (3)	0.35 (6)	0.49 (2)
TiO_2	5.50 (50)	6.45 (34)	3.99 (16)	4.05 (9)	7.46 (10)	5.56 (46)
Al_2O_3	5.69 (12)	3.83 (12)	5.74 (25)	5.08 (28)	3.36 (15)	3.60 (3)
Cr_2O_3	0.14 (1)	0.00 (0)	0.15 (1)	0.35 (10)	0.02 (1)	0.43 (28)
Fe_2O_3	52.52 (17)	51.68 (42)	56.00 (48)	54.92 (29)	51.49 (25)	55.01 (74)
FeO	30.04 (53)	34.27 (27)	31.18 (33)	30.39 (84)	32.39 (13)	30.92 (50)
MnO	0.34 (2)	0.41 (3)	0.40 (6)	0.25 (2)	0.56 (5)	0.55 (5)
MgO	3.60 (18)	1.91 (11)	2.71 (16)	2.73 (18)	3.13 (6)	3.18 (22)
CaO	0.55 (3)	0.07 (4)	0.18 (6)	0.24 (2)	0.22 (2)	0.17 (7)
Nb_2O_5	0.084 (12)	0.050 (5)	0.044 (5)	0.034 (4)	0.056 (8)	0.078 (9)
Ta_2O_5	0.051 (6)	0.048 (8)	0.042 (6)	0.053 (9)	0.052 (5)	0.024 (3)
Total	99.07 (65)	98.76 (60)	100.51 (65)	98.27 (44)	99.04 (48)	99.98 (68)
Min prop.	50 0 2 48	40 0 5 55	30 30 5 35	25 10 3 62	50 0 5 45	35 30 5 30
Glass *n*	19	21	21	29	15	6
SiO_2	57.68 (81)	62.55 (90)	55.76 (86)	61.46 (89)	61.26 (70)	59.82 (188)
TiO_2	0.36 (5)	0.36 (10)	0.26 (6)	0.25 (5)	0.70 (13)	0.27 (5)
Al_2O_3	19.21 (42)	17.78 (28)	19.14 (33)	17.87 (20)	19.45 (16)	17.71 (28)
FeO	1.49 (22)	1.80 (63)	1.56 (35)	1.61 (39)	1.58 (24)	1.51 (17)
MnO	0.13 (3)	0.11 (3)	0.15 (3)	0.09 (3)	0.13 (4)	0.17 (5)
MgO	0.06 (4)	0.19 (21)	0.07 (3)	0.15 (8)	0.06 (5)	0.20 (7)
CaO	6.96 (20)	5.86 (16)	7.09 (23)	5.62 (15)	3.73 (23)	4.74 (39)
K_2O	0.20 (2)	0.11 (2)	0.33 (6)	0.20 (4)	1.42 (13)	0.52 (6)
Na_2O	5.43 (49)	3.85 (36)	3.89 (24)	3.55 (28)	4.60 (56)	3.34 (29)
P_2O_5	0.33 (5)	0.23 (5)	0.40 (7)	0.12 (3)	0.26 (5)	0.51 (3)
Nb_2O_5	0.98 (4)	0.42 (3)	0.90 (7)	0.67 (7)	0.31 (3)	0.96 (18)
Sm_2O_3	0.28 (4)	0.15 (2)	0.25 (4)	0.27 (3)	0.12 (2)	0.28 (5)
Ta_2O_5	0.69 (5)	0.28 (3)	0.59 (5)	0.53 (7)	0.20 (3)	0.80 (6)
Total	93.80 (77)	93.69 (33)	90.39 (45)	92.39 (81)	93.82 (42)	90.83 (33)

Table 2 (continued)

	ABAYZG	478YZG	AT4YZG	557YZG	T85YZG	478YZG	AT4YZG
P (kbar)	5	5	5	5	5	2	2
T (°C)	940	940	940	940	940	940	940
Magt *n*	9	8		22	10	12	14
SiO_2	0.13 (2)	0.12 (2)	0.10 (1)	0.12 (2)	0.17 (1)	0.10 (2)	0.12 (0)
TiO_2	4.32 (10)	6.90 (32)	3.65 (5)	3.67 (2)	3.82 (29)	7.61 (56)	3.14 (21)
Al_2O_3	5.17 (19)	4.03 (7)	5.14 (14)	4.80 (8)	3.63 (17)	4.76 (17)	5.87 (32)
Cr_2O_3	0.43 (1)	0.43 (3)	0.18 (1)	0.08 (1)	0.06 (0)	0.05 (0)	0.44 (3)
Fe_2O_3	54.17 (29)	50.29 (26)	55.67 (71)	56.48 (76)	57.84 (16)	50.46 (17)	57.37 (33)
FeO	30.51 (32)	33.64 (49)	30.45 (36)	30.31 (17)	30.27 (38)	29.78 (66)	26.93 (11)
MnO	0.40 (3)	0.52 (4)	0.43 (2)	0.29 (3)	0.37 (3)	0.45 (2)	0.50 (5)
MgO	2.74 (17)	2.16 (12)	2.42 (7)	2.65 (12)	2.77 (17)	5.31 (27)	4.60 (28)
CaO	0.24 (1)	0.14 (1)	0.21 (0)	0.18 (0)	0.22 (2)	0.15 (0)	0.25 (0)
ZrO_2	0.007 (2)	0.008 (3)	0.008 (2)	0.007 (1)	0.004 (1)	0.014 (3)	0.020 (3)
Total	98.12 (49)	98.24 (87)	98.25 (27)	98.58 (52)	99.15 (44)	98.69 (61)	99.25 (71)
Min. prop.	50 0 2 48	40 0 5 55	35 25 5 35	22 15 3 60	50 0 5 45	35 30 5 30	35 30 5 30
Glass *n*	14	19	30	11	12	6	6
SiO_2	60.49 (85)	62.31 (105)	60.19 (170)	62.37 (65)	61.02 (77)	60.51 (74)	60.52 (88)
TiO_2	0.29 (10)	0.38 (15)	0.24 (6)	0.25 (4)	0.32 (13)	0.74 (12)	0.44 (8)
Al_2O_3	19.68 (21)	18.04 (22)	18.81 (54)	18.29 (18)	19.75 (39)	17.64 (34)	17.63 (44)
FeO	1.16 (28)	1.30 (22)	1.32 (23)	1.38 (12)	1.03 (26)	1.78 (29)	3.22 (84)
MnO	0.10 (3)	0.12 (2)	0.14 (4)	0.08 (3)	0.07 (2)	0.11 (2)	0.17 (4)
MgO	0.03 (2)	0.12 (9)	0.08 (9)	0.08 (2)	0.11 (20)	0.43 (23)	0.97 (67)
CaO	6.82 (23)	6.11 (21)	6.29 (25)	5.77 (19)	5.14 (35)	5.25 (27)	4.79 (42)
K_2O	0.19 (11)	0.08 (4)	0.38 (27)	0.13 (8)	0.66 (54)	0.32 (3)	1.52 (25)
Na_2O	4.18 (54)	3.78 (34)	3.65 (46)	3.72 (24)	3.88 (43)	3.17 (14)	3.45 (59)
P_2O_5	0.36 (4)	0.28 (5)	0.38 (8)	0.13 (3)	0.18 (5)	0.31(4)	0.46 (3)
Y_2O_3	0.17 (2)	0.21 (4)	0.13 (3)	0.17 (2)	0.06 (3)	0.30 (3)	0.20 (3)
ZrO_2	0.19 (3)	0.12 (2)	0.16 (2)	0.16 (3)	0.16 (3)	0.36 (0)	0.33 (4)
Gd_2O_3	0.14 (2)	0.17 (3)	0.10 (2)	0.14 (2)	0.04 (1)	0.22 (3)	0.13 (2)
Total	93.80 (73)	93.02 (85)	91.87 (39)	92.67 (51)	92.41 (66)	91.14 (74)	93.83 (37)

[a]Run at QFM-1 at Oak Ridge National Laboratory. 1σ standard deviations are presented in parentheses (e.g., 40.13 (84) equals 40.13 ± 0.84). Difference between total and 100% for glasses is assumed to be H_2O. Mineral proportions are given in the order — amphibole, plagioclase, magnetite and glass unless otherwise noted. Fe_2O_3 calculated on the basis of stoichiometry.

6-fold co-ordination. Site occupancies are complex, but the group can be divided into two categories, normal spinels, where 2+ cations occupy A and twice as many 3+ cations occupy B, and inverse spinels, where 3+ cations occupy A, and B is filled with equal amounts of 2+ and 3+ cations (Lindsley, 1976). In ulvospinels or other spinels involving 4+ cations, the 4+ cation occupies a B-site. The complexity of substitution mechanisms in magnetite doped with the HFSE makes determination of site occupancies difficult, particularly for 5+ cations such as Ta and Nb, where the substitution mechanism is unknown.

To describe partitioning behavior, the necessary information is related less to occupancy than to the mixing behavior of the end-member components. One of the prime characteristics of spinel-group phase equilibria are the large miscibility gap that exists between some of the end members. Experiments (e.g., Turnock and Eugster, 1962; Muan et al., 1972) have determined that the largest miscibility gaps exist between the Al–Cr spinels (pleonaste, hercynite, chromite) and the Fe^{3+}–Ti spinels (magnetite, ülvospinel).

4. Framework for a numerical model

Description of the relative importance of the parameters that control trace element partitioning requires that we first identify them. This issue was dealt with in Nielsen et al. (1994) by examining the data set and subsets of it for significant correlations between partition coefficients and a variety of compositional parameters. This technique has been successfully applied to a variety of systems (Lindstrom, 1976; Irving, 1978; Nielsen, 1985; Gallahan and Nielsen, 1992). However, most of these models have required that the mixing properties of the minerals be modeled in a simple fashion, usually assuming ideal

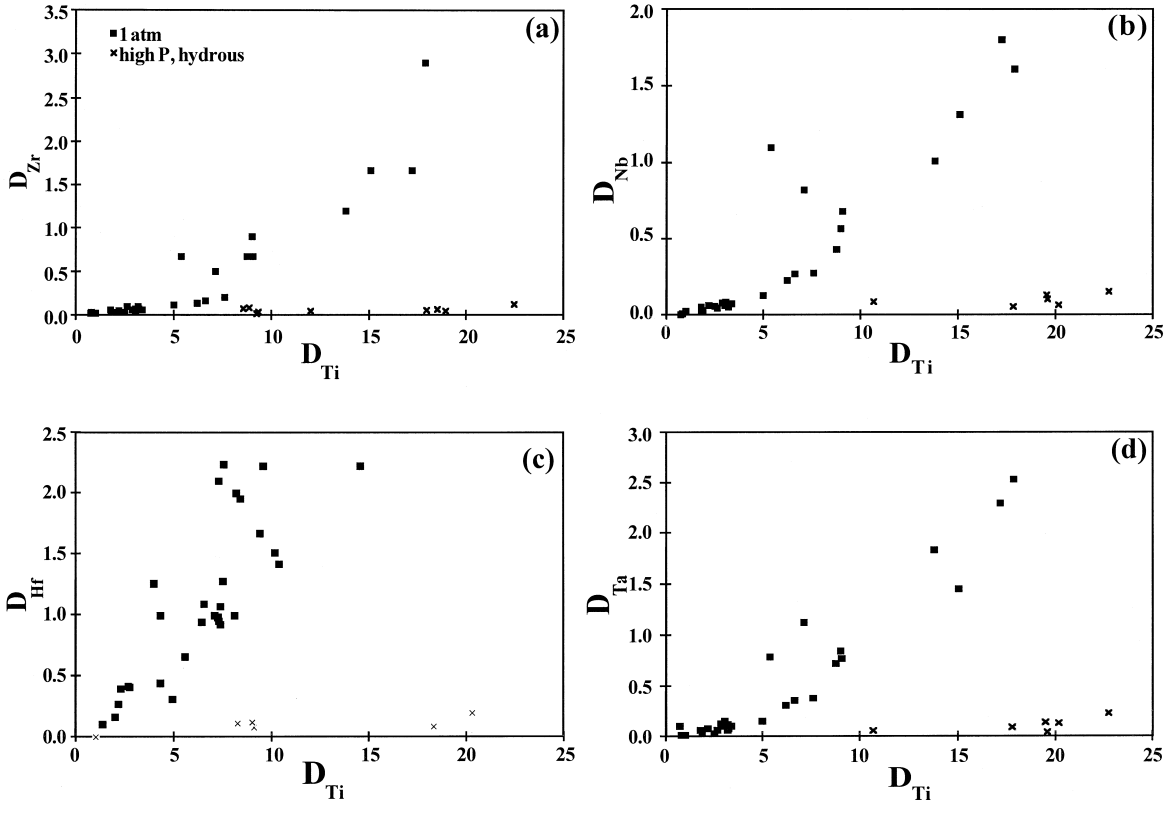

Fig. 1. Correlation of D_{HFSE} with D_{Ti}. Note the departure of the 2–5 kbar data from the trends exhibited by the 1 atm data.

mixing (e.g., Nielsen et al., 1992). This approach works because the mixing properties for many common minerals were sufficiently simple that they could be approximated as ideal if correcting parameters were added to the expressions describing partitioning (Hack et al., 1994). However, due to the simplifying assumptions of these models, their application is limited to the compositional range of their calibration dataset. For example, in pyroxene–melt systems, the thermodynamics of high-Ca clinopyroxene and low-Ca clinopyroxene require separate treatment (Gallahan and Nielsen, 1992; Nielsen et al., 1992; Hack et al., 1994; Wood and Blundy, 1997).

Though most investigators who have tried to quantify general expressions for describing partition coefficients or equilibrium constants have correlated them with temperature, many also included compositional parameters (Forsythe et al., 1994; Nielsen et al., 1994; LaTourrette et al., 1995; Wood and Blundy, 1997). In natural systems, the relationship between temperature and phase composition are complex since composition, temperature, and pressure are all interdependent variables. Since it is our primary goal to derive trace element expressions that are useful for the simulation of igneous differentiation of natural magmas, our choice of parameters is dictated by criteria other than if we were solely attempting to model the thermodynamics of this system. In particular, it is critical that the parameters used in the expressions be readily accessible, or at least be estimated by investigators.

5. Results

The most important observation noted in Nielsen et al. (1994) was the strong correlation between D_{Ti}

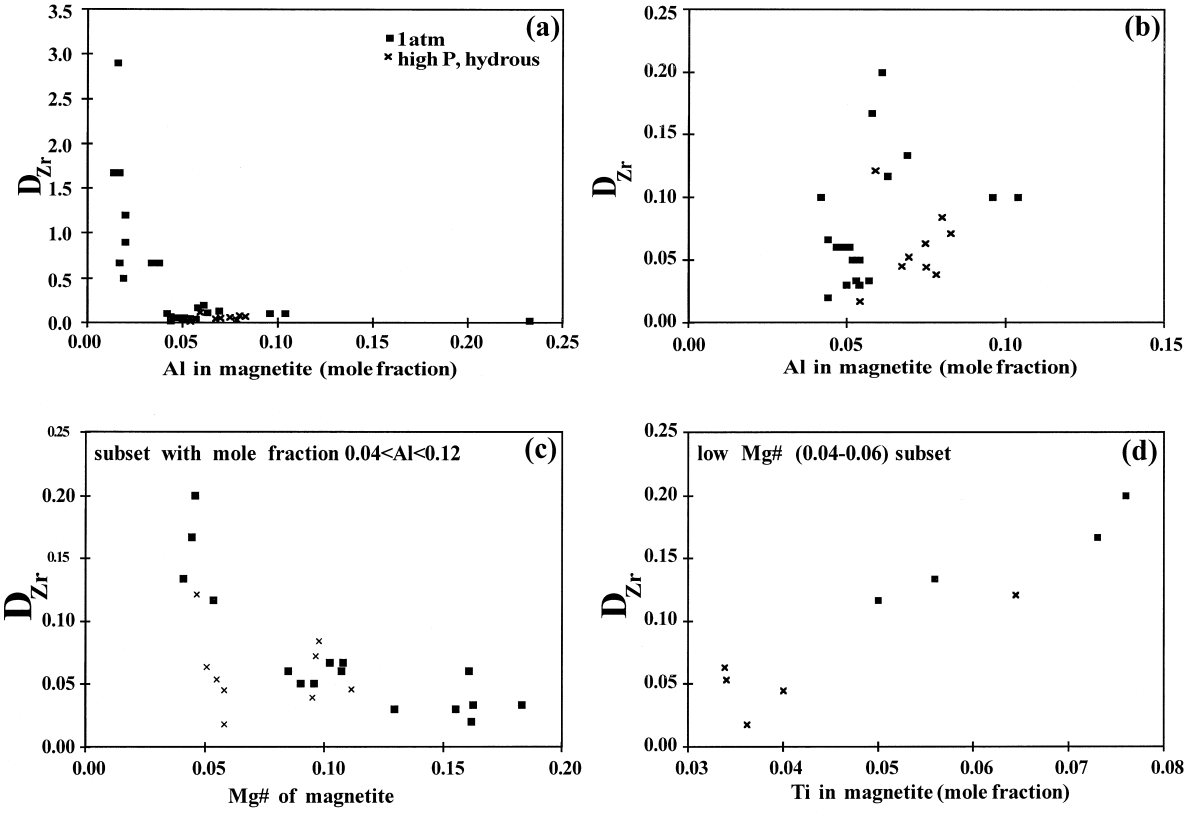

Fig. 2. Correlation of (a) D_{Zr} with Al mole fraction in magnetite. (b) Expanded view of a. (c) Correlation of D_{Zr} with Mg# of the magnetite for sub-set of intermediate values of Al in the magnetite (0.04–0.12 mole fraction). (d) D_{Zr} versus mole fraction of Ti in magnetite for a low Mg# subset of data presented in c.

and D_{HFSE}. This is in contrast to their poor correlation with temperature and pressure. The correlation of D_{HFSE} with D_{Ti} and other compositional parameters allowed expressions to be derived that could estimate D_{HFSE} for those 1 atm data. However, examination reveals that the 2–5 kbar data from this study are significantly offset from the 1 atm data (Fig. 1). This offset, present in all the trace HFSE, invalidates the expressions of Nielsen et al. (1994) for any applications at temperatures below 1000°C or to hydrous systems. This change in the relationship between Ti and the HFSE emphasizes that for the spinel group, partition coefficients are a poor representation of equilibrium constants, as one would expect based on the strong non-ideality in the mixing properties of the spinel end members (Sack and Ghiorso, 1991).

If we examine the data set in detail, we can see that the 2–5 kbar data fall into the same compositional range as the 1 atm data (Fig. 2a). From the subset of the data with molar Al in the magnetite between 4–11% (Fig. 2b), we see considerable overlap of the two data sets, and a wide range of D_{Zr} at any specific Al content. If we examine this subset of the data with respect to Mg#, we find that there is a general decrease in D_{Zr} as a function of the Mg# of the magnetite (Fig. 2c). However, there remains a significant range of D_{Zr} at any specific Mg#. Further subdividing the data and examining only the low Mg# analyses, we see that there is a linear correlation with the Ti content of the spinel (Fig. 2d). Therefore, as we continue to restrict the number of compositional variables, the variability of D_{Zr} decreases. From this we can see that all these compositional parameters are interacting, and thus must be accommodated in any quantitative model.

6. Discussion

One of the goals of most models of trace element partitioning is to relate simple measures of partitioning such as partition coefficients, to equilibrium constants. Those equilibrium constants can then be given a ''simple'' thermodynamic treatment. Owing to the large number of variables, it is difficult if not impossible, to isolate any one of the parameters and its individual effect without considering the simultaneous effects of the others. One approach useful in dealing with data sets of this type is to apply multiple linear regression using variables correlated with the controlling parameters. This approach empirically mimics an expression in which equilibrium expressions for all the endmembers are combined, and the term describing the partitioning behavior of one component is solved for.

To quantify the dependencies described above, 24 combinations of parameters were applied to the data from this study. The fewest number of parameters that yielded a goodness of fit above 0.85 were seven, including temperature, pressure, ln D_{Ti}, mol.% Al and Ti in the magnetite and Mg exchange (D_{Fe}/D_{Mg}). The resulting equations for the four HFSE are of the form:

$$\begin{aligned}\ln D_{HFSE} = {} & C_0 + C_1 \ln D_{Ti} + C_2(\text{Ti in magnetite}) \\ & + C_3(\text{Al in magnetite}) \\ & + C_4(\text{Mg exchange}) \\ & + C_5(\text{Ti}/\text{Al in magnetite}) \\ & + C_6 P(\text{kbar}) + C_7(10\,000/T(\text{K}))\end{aligned}$$

where C_0, C_1, C_2, C_3, C_4, C_5, C_6 and C_7 are regression constants (Table 3) and the compositional parameters are calculated as cation normalized mol.%. The internal precision of these expressions was calculated by applying the expressions listed in Table 3 to the calibration data set. Ds for the Zr, Nb, Hf and Ta are predicted to within 40–50% (relative; 1σ) over a total range of nearly two orders of magnitude (Ds from < 0.1 to > 3) (Fig. 3a–d). If we examine the regression constants, Ti and D_{Ti} have the greatest influence on the calculated D_{HFSE}. However, each of the other parameters have a significant impact, but the impact is restricted to different parts of the data set. For example, D_{HFSE} for high Al spinels is strongly suppressed by the Al and Al/Ti terms, and in most cases by the Mg exchange, due to the fact that most high Al magnetites are also high Mg, and have high D_{Mg} relative to D_{Fe}. This makes it difficult to reduce the number of controlling parameters.

As an independent check, we applied the regressions to the data of Horn et al. (1994), which were not included in the calibration data set. Those data

Table 3
Regression constants for expressions describing the magnetite-melt partition coefficients of Zr, Nb, Hf, and Ta
Equation is in the form: $\ln D_{HFSE} = C_0 + C_1 \ln D_{Ti} + C_2$ (Ti in magnetite) + C_3 (Al in magnetite) + C_4 (Mg exchange in magnetite) + C_5 (Ti/Al in magnetite) + C_6 (P) + $C_7(10\,000/T$ (K)).
All terms are calculated in terms of cation normalized mole fractions. Mg exchange = $D_{Fe^{+2}}/D_{Mg}$ where Fe^{+2} in magnetite has been calculated on the basis of stoichiometry. Internal precision presented in terms of 1σ reproducibility (100* calculated D/experimental D).

	ln D_{Ti}	Ti	Al	Mg ex	Ti/Al	P (kbar)	$10\,000/T$ (K)	C_0	Reprod. (%)	R^2
ln D_{Zr}	1.89 (31)	−2.40 (98)	−3.56 (87)	3.03 (18)	0.058 (7)	−0.30 (5)	−1.89 (27)	8.65 (33)	40	0.93
ln D_{Nb}	1.85 (23)	−6.27 (76)	−5.45 (65)	3.38 (26)	0.069 (9)	−0.32 (3)	−1.45 (21)	6.07 (37)	38	0.92
ln D_{Hf}	1.83 (37)	−5.46 (180)	−5.42 (56)	3.27 (31)	0.072 (5)	−0.31 (2)	−1.59 (18)	8.03 (25)	51	0.90
ln D_{Ta}	2.34 (41)	−7.41 (110)	−5.62 (37)	3.53 (24)	0.075 (8)	−0.35 (6)	−1.74 (23)	7.93 (19)	45	0.89

were produced at relatively high temperature (1235–1275°C) at 1 atm pressure under oxidizing conditions (> Ni–NiO or in air). The liquid compositions are basaltic, and generally more magnesian than those of Nielsen et al. (1994). The magnetite compositions are also more magnesian, and several contain significant Cr. These data are therefore significantly different in the critical parameters that control partitioning.

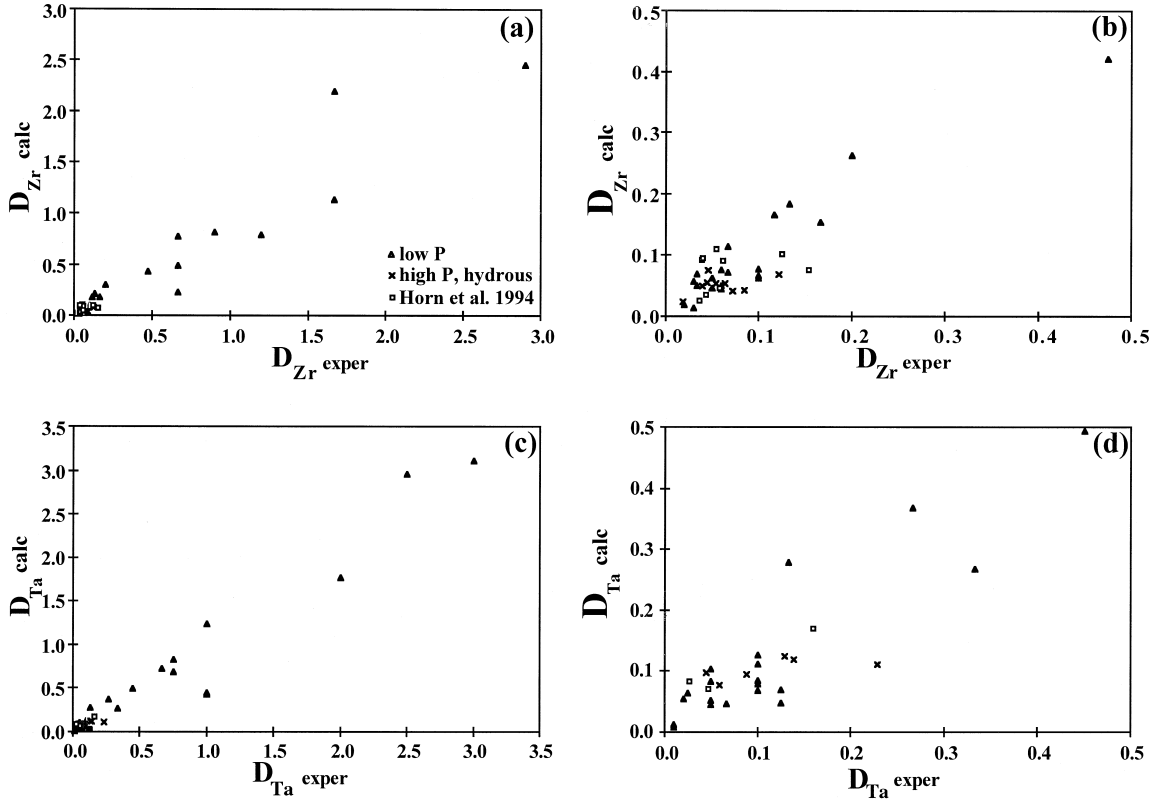

Fig. 3. Correlation of partition coefficients measured from the experimental charges (exper) with values calculated from the expressions in Table 3 using the experimental liquids as unknowns (calc). b and d are expanded scale versions of a and c, respectively.

They were not included in the calibration data set because the experimental conditions under which they were formed (high f_{O_2}) is significantly outside the conditions under which most magnetite form in nature.

This comparison with independent data is critical because of the large number of terms in the expression, and the potential that data outside the calibration dataset will generate calculated partition coefficients significantly different from the experimental values. The results are generally within the 20–40% analytical error associated with the data (Fig. 3a–d), not greatly above the cited analytical error for those determinations. Equally important, the calculated numbers fall within the calibration data set, suggesting no systematic bias. Therefore, expression (3) successfully models the effects of the differences in composition, partition coefficients, temperature and f_{O_2}. It is general knowledge that the effect of increasing f_{O_2} is to stabilize magnetite at higher temperature. However, if one considers the Horn et al. (1997), the other effect is to produce magnetites that are high in Fe^{3+} and Al and Cr, compared to magnetites produced at lower temperatures from more evolved magmas. The experimental results of Horn et al. (1997), plus the calculated parameters calculated above, indicate that the net effect will be for D_{HFSE} to be low for most high f_{O_2} conditions, particularly during the initial stages of crystallization.

The negative correlation of D_{HFSE} with Al mole fraction in magnetite is consistent with the observed miscibility gap that exists between $(Fe, Mg)_2TiO_4$ and $(Mg, Fe)Al_2O_4$ (Muan et al., 1972). Since Ti is excluded from Al-rich spinel group minerals, it is likely that other high valence cations would also be excluded. The relatively higher D_{HFSE} in spinels with equivalent Ti content but lower Mg# indicates that they are influenced by the wider miscibility gap characteristic of Mg_2TiO_4–$MgAl_2O_4$ compared to Fe_2TiO_4–$FeAl_2O_4$ (Turnock and Eugster, 1962).

Based on 1 atm data alone, Nielsen et al. (1994) concluded that D_{HFSE} is more sensitive to the composition of the spinel than is D_{Ti}. This can be seen in the shallow slope of the D_{HFSE} vs. D_{Ti} correlation at low D_{Ti} (Fig. 1). We interpreted this observation as evidence that the miscibility gap between HFSE-ulvospinel and Mg–Al–Cr rich spinels is wider than for Ti-ulvospinel and Mg–Al–Cr-rich spinels (i.e., more strongly non-ideal). If we examine the changes in the Onuma curves (Onuma et al., 1968) for these elements as a function of temperature (Fig. 4), we can further see that the difference in the miscibility gap increases with decreasing temperature. Comparison of data from two experiments with similar D_{Ti}, one at 1 atm and high temperature (V-31), and another at 2 kbar and low temperature (478), illustrates the change in the shape of the relationship between ionic radius and partition coefficient described by the lines linking the 4+ cations. Further, data from the high temperature experiments of Horn et al. (1994) has an even shallower slope for the 4+ cations, indicating that the site becomes more accepting of the larger trace cations Zr and Hf (relative to Ti) at high temperature. With decreasing temperature, the structure becomes increasingly exclusive of the HFSE relative to Ti.

Theoretically, the approach of LaTourrette et al. (1995) and Wood and Blundy (1997) could be used to estimate the partition coefficients of the trace cations from a knowledge of the stress parameters and the partitioning behavior of Ti. However, the complexity of the compositional dependence of partitioning behavior in spinels documented above makes it unrealistic to calibrate the required expression from the existing small database.

Our results therefore imply that magnetite–melt partition coefficients are predominantly dependent on mineral composition. We believe that the role of variation in melt component activities are a contributing factor; however, the nature of the mixing properties of spinels dominates. For example, if we consider the 2–5 kbar experiments, those melts are generally higher in silica than the 1 atm experiments. However, if the change in slope of the Onuma curves were due to melt composition, one would expect both D_{HFSE} and D_{Ti} to increase together, which do not (Figs. 1 and 2).

The key finding of this work is that our results imply that the effects of either residual or fractionating magnetite on HFSE abundances in hydrous, silicic magmas will be small to the point of being undetectable. This is particularly true given that amphibole–melt and pyroxene–melt partitioning coefficients for HFSE are elevated in such magmas (Forsythe et al., 1994; Hilyard et al., submitted) and that

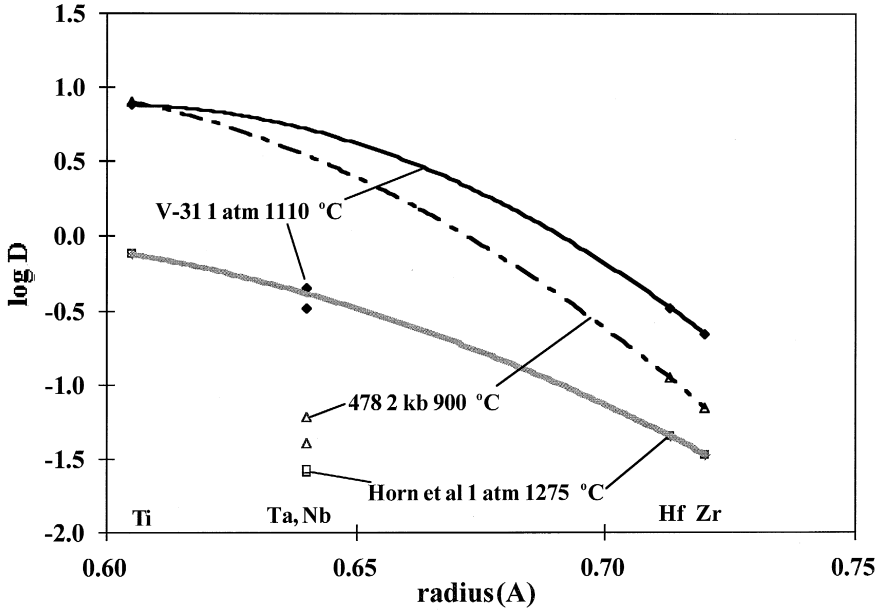

Fig. 4. Correlation of partition coefficient with ionic radius (Onuma diagram). Three cases illustrated include data from mafic, high f_{O_2}, high temperature, 1 atm (Horn et al., 1994), Fe-rich intermediate temperature, 1 atm (V-31) and low temperature, 2 kbar (478). Note the increasingly steep relationship between D_{Ti} and D_{Hf} and D_{Zr} with decreasing temperature. Ionic radii are from Shannon (1976).

HFSE-bearing minerals (e.g., zircon, allanite) may be present. Even the most extreme situations, for example, the assimilation of large amounts (10%) of pure magnetite by a basalt in equilibrium with Uv65 magnetite, result in a net decrease of Nb and Zr of only about 10% relative, while reducing Ti by 50–75%. Moreover, even this extreme (and unlikely) situation will not influence ratios of trace HFSE (e.g., Nb/Zr).

The complexity of spinel-group mineral chemistry, as well as the dependence of the activity-composition relations on temperature and pressure suggests that robust description of magnetite–melt partitioning will require additional experimental data on intermediate temperatures and compositions. Nevertheless, the results reported here will allow us to better plan those additional experiments.

7. Conclusions

The partitioning behavior of the HFSE is controlled by the major element composition of the magnetite. These controls are consistent with our understanding of the mixing properties of the spinel group, where HFSE partition preferably into Ti, Fe^{3+}-rich, Al, Cr-poor magnetites. Because the controls are dominated by the mineral composition, the *D*s for the HFSEs are similar to one another over a range of two orders of magnitude.

The wide range of partitioning behavior and the magnitude of the compositional dependence exhibited in our new data set illustrates the need to take great care when building petrogenetic models. Specifically, if applied to low temperature, 2–5 kbar data, the expressions of Nielsen et al. (1994) will produce results that are approximately a factor of 5–10 too high. New expressions including terms for the concentration of Ti and Al should be more robust. This is supported by their application to an independent data set whose composition is significantly different from the calibration data (Horn et al., 1994).

Magnetite will have a small effect on the HFSE budget for most silicic systems in the presence of significant water because of the resultant low temperature and aluminous liquids. This is particularly true since HFSE partition coefficients for amphibole

and pyroxene are highest under those same conditions (Forsythe et al., 1994; Hilyard et al., submitted). Nevertheless, the sensitivity of D_{HFSE} to changes in composition means that in any environment where contrasting conditions prevail, small changes in composition of the equilibrium magnetite can substantially change the bulk partition coefficient of the HFSE. The similarity of the D_{HFSE}s means that magnetite fractionation may affect the absolute abundance of these elements, but not their ratios (e.g., Nb/Zr)

Acknowledgements

We would like to thank all of those who graciously supplied starting materials and advice when we were setting up this investigation: Bill Leeman, Roz Helz, John Sinton, Tom Wright, Mike Rhodes, Don Baker, Bill Melson and Dave Christie. We would especially like to thank Bob Bodnar and Jim Student at Virginia Polytechnic, Jim Blencoe at Oak Ridge National Lab and Alberto Patiño Douce at the Univ. of Georgia for providing access to their equipment, without which this project would have been impossible. We would also like to thank Trevor Green and John Blundy for thorough and constructive reviews. This investigation was supported by NSF grant EAR9406134 to RLN and EAR9405266 to JSB. *[MB]*

References

Anderson, A.T., 1974. Before eruption H_2O content of some high alumina magmas. Bull. Volcanol. 37, 530–552.

Beard, J.S., Lofgren, G.E., 1991. Dehydration Melting and water-saturated melting of basaltic to andesitic greenstones and amphibolites at 1, 3, and 6.9 kbar. J. Petrol. 32, 365–401.

Beattie, P., 1993. On the occurrence of apparent non-Henry's Law behavior in experimental partitioning studies. Geochim. Cosmochim. Acta 57, 47–55.

Drake, M.J., Holloway, J.R., 1981. Partitioning of Ni between olivine and silicate melt: the ''Henry's Law problem'' reexamined. Geochim. Cosmochim. Acta 45, 431–437.

Drake, M.J., Weill, D.F., 1972. New rare earth element standards for electron microprobe analysis. Chem. Geol. 10, 179–181.

Duncan, R.A., Fisk, M.R., White, W.M., Nielsen, R.L., 1995. Tahiti: geochemical evolution of a French Polynesian Volcano. J. Geophys. Res. 99 (B12), 24341–24357.

Forsythe, L.M., Nielsen, R.L., Fisk, M.R., 1994. The partitioning of HFSE between pyroxene and natural mafic to intermediate composition silicate liquids at 1 atm to 10 kbar. Chem. Geol. 117, 107–125.

Gallahan, W.E., Nielsen, R.L., 1992. Experimental determination of the partitioning of Sc, Y and REE between high-Ca clinopyroxene and natural mafic liquids. Geochim. Cosmochim. Acta 56, 2387–2404.

Garcia, M.O., Liu, N.W.K., Muenow, D.W., 1979. Volatiles in submarine volcanic rocks from the Marianas island arc and trough. Geochim. Cosmochim. Acta 43, 305–312.

Gill, J.B., 1978. Role of trace element partition coefficients in models of andesite genesis. Geochim. Cosmochim. Acta 42, 709–724.

Hack, P.J., Nielsen, R.L., Johnston, A.D., 1994. Experimentally determined rare-earth element and Y partitioning behavior between clinopyroxene and basaltic liquids at pressures up to 20 kbar. Chem. Geol. 117, 89–105.

Hilyard, M., Nielsen, R.L., Beard, J.S., Patiño-Douce, A., Blencoe, J., submitted. Experimental determination of the partitioning behavior of rare earth and high field strength elements between pargasitic amphibole and natural silicate melts. Geochim. Cosmochim. Acta.

Horn, I., Foley, S.F., Jackson, S.E., Jenner, G.A., 1994. Experimentally determined partitioning of high field strength- and selected transition elements between spinel and basaltic melt. Chem. Geol. 117, 193–218.

Irving, A.J., 1978. A review of experimental studies of crystal/liquid trace element partitioning. Geochim. Cosmochim. Acta 42, 743–770.

Jarosewich, E., Nelen, J.A., Norberg, J.A., 1980. Reference samples for electron microprobe analysis. Geostandards Newslett. 4, 43–47.

Kelemen, P.B., Johnson, K.T.M., Kinzler, R.J., Irving, A.J., 1990. High field strength element depletions in arc basalts due to mantle–magma interaction. Nature 345, 521–524.

LaTourrette, T.Z., Burnett, D.S., Bacon, C.R., 1991. Uranium and minor-element partitioning in Fe–Ti oxides and zircon from partially melted granodiorite, Crater Lake, OR. Geochim. Cosmochim. Acta 55, 457–469.

LaTourrette, T., Hervig, R.L., Holloway, J.R., 1995. Trace element partitioning between amphibole, phlogopite, and basanite melt. Earth Planet. Sci. Lett. 135, 13–30.

Lemarchand, F., Villemant, B., Calas, G., 1987. Trace element distribution coefficients in alkaline series. Geochim. Cosmochim. Acta 51, 1071–1081.

Lindstrom, D.J., 1976. Experimental study of the partitioning of the transition metals between clinopyroxene and coexisting silicate liquids. PhD thesis, Univ. of Oregon, Eugene, 188 pp.

Lindsley, D.H., 1976. The crystal chemistry and structure of oxide minerals as exemplified by the Fe–Ti oxides. In: Rumble, D. (Ed.), Oxide Minerals, MSA Reviews in Mineralogy, Vol. 3, 1–52.

Michael, P.J., 1988. Partition coefficients for rare earth elements in mafic minerals of high silica rhyolites: the importance of accessory mineral inclusions. Geochim. Cosmochim. Acta 52, 275–282.

Muan, A., Hauck, J., Lofall, T., 1972. Equilibrium studies with a bearing on lunar rocks. Proc. 3rd Lunar Sci. Conf., pp. 185–196.

Nielsen, R.L., 1985. A method for the elimination of the compositional dependence of trace element distribution coefficients. Geochim. Cosmochim. Acta 49, 1775–1779.

Nielsen, R.L., Gallahan, W.E., Newberger, F., 1992. The partitioning of Sc, Y, and the REE between olivine, low-Ca pyroxene, ilmenite, magnetite and natural silicate magmas. Contrib. Mineral. Petrol. 110, 488–499.

Nielsen, R.L., Forsythe, L.M., Gallaghan, W.E., Fisk, M.R., 1994. Major and trace element magnetite–melt partitioning. Chem. Geol. 117, 167–191.

Nielsen, C.H., Sigurdsson, H., 1981. Quantitative methods for electron microprobe analysis of sodium in natural and synthetic glasses. Am. Mineral. 66, 547–552.

Onuma, N., Higuchi, H., Wakita, H., 1968. Trace element partition between two pyroxenes and the host volcanic rocks. Earth Planet. Sci. Lett. 5, 47–51.

Patiño-Douce, A.E., Beard, J.S., 1995. Dehydration melting of biotite gneiss and quartz amphibolite from 3 to 15 kbar. J. Petrol. 36, 707–738.

Patiño-Douce, M.L., Patiño-Douce, A., Qayyum, M., Nielsen, R.L., 1994. A new set of low concentration standards for La, Ce, Sm, Yb, Lu, Y, Sc, V, Nb, and Ta in silicates. Geostandards Newslett. 18, 195–198.

Rushmer, T., 1991. Partial melting of two amphibolites: contrasting experimental results under fluid absent conditions. Contrib. Mineral. Petrol. 107, 41–59.

Sack, R.O., Ghiorso, M.S., 1991. An internally consistent model for the thermodynamic properties of Fe–Mg titanomagnetite aluminate spinels. Contrib. Mineral. Petrol. 106, 474–505.

Shannon, R.D., 1976. Revised effective ionic radii and systematic studies of interatomic distances on halides and chalcogenides. Acta Crystal. 32, 751.

Sisson, T.W., Grove, T.L., 1993. Experimental investigations of the role of H_2O in calc-alkaline differentiation and subduction zone magmatism. Contrib. Mineral. Petrol. 113, 143–166.

Turnock, A.C., Eugster, H.P., 1962. Fe–Al oxides: phase relations below 1000°C. J. Petrol. 3, 533–565.

Villemant, B., 1988. Trace element evolution in the Phlegrean Fields, Central Italy: fractional crystallization and selective enrichment. Contrib. Mineral. Petrol. 98, 169–183.

Villemant, B., Jaffrezic, J., Joron, J., Treuil, M., 1981. Distribution coefficients of major and trace elements: fractional crystallization in the alkali basalt series of Caine de Pus, Massif Central, France. Geochim. Cosmochim. Acta 45, 1997–2016.

Watson, E.B., 1985. Henry's Law behavior in simple systems and magmas: criteria for determining concentration-dependent partition coefficients in nature. Geochim. Cosmochim. Acta 49, 917–923.

Wood, B.J., Blundy, J.D., 1997. A predictive model for rare earth element partitioning between clinopyroxene and anhydrous silicate melt. Contrib. Mineral. Petrol. 129, 166–181.

Worner, G., Beusen, J.M., Duchateau, N., Gijbels, R., Schmincke, H.U., 1983. Trace element abundances and mineral/melt distribution coefficients in phonolites from the Laacher See Volcano, Germany. Contrib. Mineral. Petrol. 84, 152–173.